Exploring the potential of electrostatic precipitation as an alternative particulate matter filtration system in aircraft cabins

Bastien Pellegrin, Philippe Berne, Hervé Giraud, Arthur Roussey

This is the pre-peer reviewed version of the following article:
Pellegrin, B, Berne, P, Giraud, H, Roussey, A. Exploring the potential of electrostatic precipitation as an alternative particulate matter filtration system in aircraft cabins. Indoor Air. 2022; 32:e12990.,
which has been published in final form at https://doi.org/10.1111/ina.12990. This article may be used for non-commercial purposes in accordance with Wiley Terms and Conditions for Use of Self-Archived Versions.

Exploring the potential of electrostatic precipitation as an alternative particulate matter filtration system in aircraft cabins

Bastien Pellegrin[1a], Philippe Berne[1], Hervé Giraud[1], Arthur Roussey[1]

[1] Univ. Grenoble Alpes, CEA, Liten, DTNM, 38000 Grenoble, France
[a] Corresponding Author: bastien.pellegrin@cea.fr

ABSTRACT

On modern airliners, cabin air pressurization, heating and renewal is achieved using air supplied from the gas turbine engines during flight. This air intake impairs the motors yield and needs to be conditioned, leading to energy overconsumption. Recent advances in thermal management enable aircraft manufacturers to reduce further the intake airflow needed to maintain cabin temperature at high altitude. Nevertheless, for lower air renewal rates, an appropriate air filtration system will be needed to maintain acceptable air quality in the cabin. In this context, Clean Sky 2 Joint Undertaking (CS2JU) project EC2S (Environment Control Secondary System) aims at developing an integrated filtration system to be implemented in existing cabin air management systems (so called Environmental Control System – ECS). The EC2S unit will include three filtration units addressing separately Volatile Organic Compounds (VOCs), CO_2 and Particulate Matter (PM). Circulated air in the ECS is conventionally filtered on pleated HEPA filters that generate substantial pressure drop. Since the EC2S VOCs and CO_2 filtration units would generate additional pressure drop in the ECS system, electrostatic precipitation is foreseen as a low flow resistance alternative for PM removal. This paper reports the development and performance assessment of a two-stage electrostatic precipitator (ESP) designed for aircraft recirculated air filtration. The ESP prototype presents single pass high particle collection rates (i.e. over 90% for airborne particles with an aerodynamic diameter of 0.5 µm or larger), low pressure drop (i.e. 4 Pa at nominal flowrate) and a limited ozone generation rate (i.e. below 8 $mg.h^{-1}$).

Keywords: *Aircraft air quality management, Electrostatic precipitation, Spectral collection efficiency, Ozone generation*

INTRODUCTION

Cabin air management system

Over the last few decades, significant efforts have been made by aircraft manufacturers to reduce the overall energetic consumption of aircraft engines. Besides providing thrust and electric power, an engine must also provide pressurized fresh air to the cabin. A substantial part of the outside air compressed by the engine is "bled" off the engine and passed through air conditioning packs to be cooled and supplied to the cabin. This "bleed-air" pressurizes and heats the cabin to overcome extreme external conditions (low temperature and pressure at high altitudes). As passengers and crew are confined in the relatively low volume of the aircraft cabin, a high flow of fresh air must be provided to the cabin. To reduce demand of bleed air on the engine for cabin thermalization and pressurization, aircraft manufacturers implemented an air recirculation system, which mixes bleed-air with air recirculated from the cabin with a recirculation fan (Figure 1). Nowadays, on most commercial airliner models, the air flowing in the cabin comprises between 30% and 50% of recirculated air [1]. Modern aircraft recirculation systems include a filtration unit which comprises a High Efficiency Particulate Air (HEPA) filter with stated single pass PM removal efficiencies up to above 99% [2]. Optionally the HEPA filters may be coupled with Activated Carbon (AC) layers to remove VOCs from recirculated air.

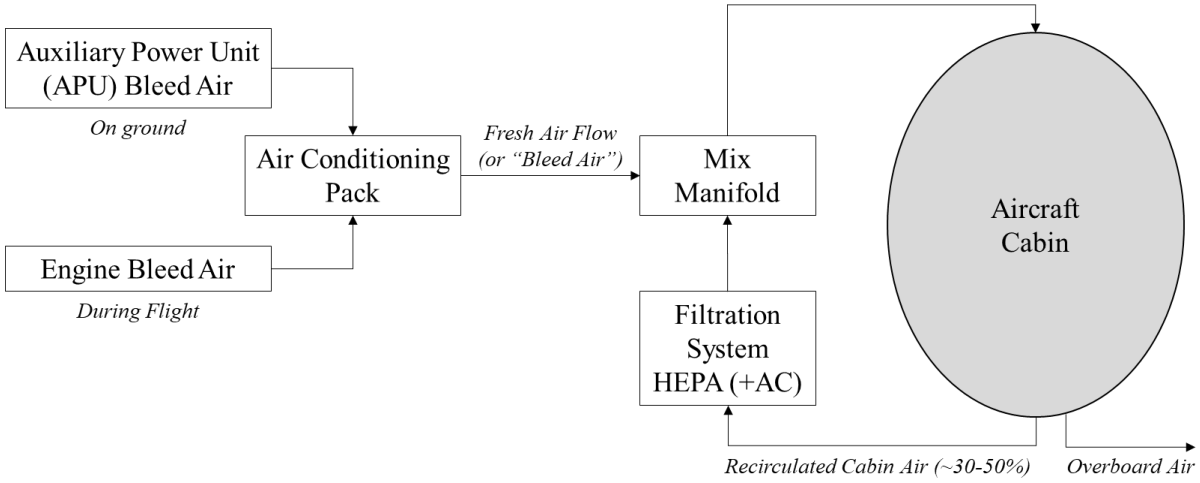

Figure 1. Simplified flow chart of a typical air supply on commercial aircraft, including a High Efficiency Particulate Air filter (HEPA) sometimes combined with an Activated Carbon (AC) filter in the recirculation loop of the ECS.

Cabin air pollution

Cabin Air Quality (CAQ) is impacted by multiple pollution sources which may be internal or external depending on aircraft position and activity on ground (maintenance, taxiing and idling periods) or during flight phases.

On the ground, in the vicinity of airport aprons and runways, the aircraft main engines combustion appears to be a predominant emission source for PM (and gaseous air pollutants such as NO_x, CO, VOCs or SO_2) [3]. Based on onsite concentration measurements, several studies estimated the PM emissions directly attributed to aircrafts in different international

airports: depending on the airport capacity, results ranged from 3.5 up to 71.5 tons per year [4-6]. Yang et al. estimated that the aircraft engines emissions account for almost 50% of fine particles ($PM_{2.5}$) concentration recorded at Beijing airport, the rest being mostly attributed to other diesel or gasoline vehicles, fuel related activities and aircraft landing or braking [6]. Some recent studies [7-10] specifically focused on the nano-sized fraction of PM, i.e. ultrafine particles (UFPs, with diameter below 100 nm). They reported the emission by the aircrafts engines of a characteristic non-volatile nano-aerosol composed of soot and other components including zinc, aluminum, and titanium. Those non-volatile UFPs were found to present a particle size distribution (PSD) with a mode at 20 nm, notably smaller than typical PSD that can be monitored in urban locations [10]. Additionally, the formation of a secondary, volatile nano-aerosol, with a mode below 10 nm (nucleation mode), originating from conversion processes of sulfur and various organic gases, was also reported [3]. Since the intake air is usually not filtered before entering the cabin, the presence of high levels of airborne particles on airport area (reaching up to 10^7 particles.cm^{-3} within runways vicinity [11]) may drastically impair the CAQ when airplanes are operated at ground level.

After take-off, air from higher altitude is provided to the aircraft cabin, and is considered to be clean, with a very low PM and UFPs concentrations (~50 particles.cm^{-3}) [12]. Similarly, at high altitudes, VOCs are present at even lower concentrations than in typical outdoor air (<10 ppb), as they are oxidized by highly reactive radicals [13]. Ozone is also present in the atmosphere, and its concentration depends on cruising altitudes. Typical concentrations are ~0.03 ppm at sea level, ~0.1 ppm at 40 000 ft (12.2 km) and ~5 ppm at 50 000 ft (15.5 km), but ozone concentrations depend also on aircraft routes and encountered weather [14]. For example, ozone-rich transients up to 0.5 ppm have been measured in the upper troposphere between 10 and 12 km [15]. Therefore, after take-off, outdoor air can be considered as clean, only containing potentially high ozone concentration.

In addition to outside air quality, internal pollution sources such as engine fluid leaks (fume events) or passengers and their activities may have an impact on CAQ. Malfunction of the air compressing system on the aircraft engine may lead to the dispersion of potentially harmful engine fluids (oil, anti-icing fluid…) in the cabin. This incidental situation, commonly referred to as fume event, is well known and documented [16-17]. It may lead to gas phase or mist pollution of the cabin with engine oil which comprises hazardous chemicals such as organophosphates (OPs) [18]. Besides fume events, passengers themselves (and their activities) represent the major pollution source during flight. Wang et al. estimated that nearly 30% of VOC concentrations in aircraft cabins were due to services and humans [19]. Cao et al. recently showed a higher particle concentration in the cabin during boarding and deplaning of a retired aircraft. They even proposed an emission rate of PM_{10} per passenger of ~15 µg.m^{-3}.pax^{-1} during boarding/deplaning, and ~5-6 µg.m^{-3}.pax^{-1} while sitting [20]. Finally, passengers are also a source of bioaerosol. As reviewed in reference [19], concentrations of airborne bacteria and fungi were however found to be generally lower than those common in indoor air.

Based on the above considerations, CAQ will highly depend on the aircraft mission and will be particularly impacted by its ground time: as fresh air is not directly filtered and enters the cabin before a first filtration (Figure 1), contaminated air will enter the cabin if the pollution sources are located outside the aircraft. Several studies were conducted on UFPs and PM concentrations in aircraft cabin and confirmed this trend [21-26]. Recorded UFPs concentrations were found to be low at high altitude (50-100 p.cm^{-3}) [21,23] and higher during on-ground operations such as taxiing (10^3-10^4 p.cm^{-3}) [23].

Cabin air filtration

According to the Federal Aviation Administration (FAA Title 14) and the American National Standards Institute (ANSI/ASHRAE standard 161), air filters are mandatory to be mounted on all commercial aircrafts. Nowadays, modern airliners ventilation systems are equipped with HEPA filters as standard [27]. The HEPA cabin air filters definition in aerospace industry is based on a minimum removal efficiency of 99.97 % when tested using a DOP challenge (mean size 0.3 µm, according to ASTM publication D 2986-95 – Boeing criteria) or 99.99 % when tested with a sodium chloride challenge (mean size 0.58 µm, according to British Standard BS.3928 – Airbus criteria) [1,28]. Typical ECS HEPA filters dimensions are roughly about 60 cm by 60 cm, with a 15-20 cm thickness and weight approximately 3-6 kg. This thickness accommodates the pleated structure of the filter medium, which substantially increases the available filter area within the 60 by 60 cm frame, reducing the pressure required to force the air through the filter. No regulation currently enforces the replacement frequency of used filters but various airliners' maintenance manuals mention a service life ranging from 3 000 to 6 000 flight hours [27,28].

Very limited scientific information is available in the literature on performance assessment of HEPA filters dedicated to filtration of airplane cabin air. Xu et al. [27] reported a comparative study of two commercially available HEPA filters from Pall (Model CD00973F2) and Donaldson (Model KK2972941) made of glass fibrous media. Pristine filters, when challenged at their respective nominal flowrates (1970 $m^3.h^{-1}$ and 1600 $m^3.h^{-1}$), exhibited pressure drop (ΔP) of approximately 280 Pa for Pall filter and 100 Pa for Donaldson filter. The efficiency of Donaldson filter (assessed according to European norm EN 1822 protocol) was shown to be 86 %, for a Most Penetrating Particle Size (MPPS) of 150 nm. For the Pall filter, a 99 % efficiency was observed for a MPPS of 55 nm. The MPPS value of the Pall filter is lower than values commonly reported in the literature for HEPA filters, which are usually in the range of 120 nm to 300 nm [29], most probably due to the presence of electrostatic charges on the media. Xu et al. [27] additionally investigated the changes of filters characteristics along with filter usage. Due to fouling, for an equivalent of 6 000 flight hours, Donaldson filter efficiency increased by 10 % (reaching 97%) and ΔP increased by 800 % (reaching 950 Pa). A recent study from Cao et al. [20] monitored the particle deposition in ECS of commercial airliners. Based on PM concentration monitored in various airports and the relationship established by Xu et al. [27] between dust loading and pressure drop, they calculated an estimated HEPA lifespan as low as 800 flight hours for aircraft operated in highly polluted airports in China (considering that the filter needs to be replaced when ΔP reaches a level that is twice the initial resistance).

ESP as an alternative to HEPA

Electrostatic precipitation (ESP) is a process to remove particulate matter in a gas using electrostatic force. ESP acts by imparting charge on airborne particles, which, in the presence of an electric field, are then directed to and deposited on a metallic collection plate [30]. It has been widely used in industry since the beginning of the 20th century for fume filtration. ESP plays a prevailing role in high flowrate atmospheric waste treatment for major sectors such as metalworking and chemical industries, cement production plants and coal-fired power plants [31], applications which operate at temperatures too high for fiber-based filters.

In the field of aerosol filtration in indoor air, the prevailing technology is the mechanical filtration on fibrous media. Nevertheless, the energy consumption of fiber based air filtration systems mainly depends on the density of the fibrous filter: the denser the filter mesh, the higher the pressure drop is. To overcome higher pressure drop, fans need to operate at higher speeds, therefore consuming more energy [32]. Additionally, throughout its life, the fibrous filter collects particles that accumulate on fibers' surface, gradually blocking the pores. This particle accumulation leads to higher collection efficiency but simultaneously generates higher pressure drop over the lifespan of the filter. This pressure drop increase requires the filter to be replaced periodically to avoid energy overconsumption or damages on the air circuit. This is why selection of a fibrous filter needs to be a trade-off where the filter is dense enough to capture the required percentage of particles while being open enough to be economically viable.

In contrast, with airflow occurring tangentially to the collection surfaces, ESP is characterized by low-pressure drop and, subsequently, has lower power requirement than its fibrous counterparts. Generally speaking, ESP may be considered less efficient in removing particles from air stream than HEPA filters when very high collection is intended (>99.9%) [33]. However, the usefulness of ESP technology in mitigating both biological and non-living aerosols has been demonstrated, even for ultrafine particles. Regarding biological matter, it is well documented that mechanical filtration may present a risk of contamination and proliferation because the surface of fibrous filters, where microorganisms and nutriments accumulate, can represent a suitable ecosystem for microorganisms growth [34,35]. For ESP, research has shown that electrical charging could impair the survival rates of bacterial cells and spores, thus limiting their proliferation [36,37]. Consequently, over the last decade, ESP have gained increasing attention for the removal of particulate matter (mainly dust particles and airborne microorganisms) in confined indoor spaces [38-40].

This study reports the sizing, design and performances assessment (single-pass collection efficiency, pressure drop and ozone emission rate) of an ESP prototype dedicated to aircraft cabin air filtration. The potential benefit of substituting HEPA filters for ESP is discussed.

METHODS

ESP Prototype

Figure 2 presents a simplified schematic of the developed ESP prototype. The device comprises two distinct sections: the charging stage and the collection stage.

The charging stage (where airborne particles acquire electric charges) operates using unipolar ions generated by corona discharge. Corona discharge is an operational condition in which a dense cloud of free electrons and unipolar ions is established around a discharge electrode. This complex phenomenon originates from a strong, non-uniform electric field, generated by high potential gradients on curved electrodes (such as wire, tip or sharp blade geometries). A simple geometry to enable corona discharge is the wire-plate geometry: a potential difference is applied between a low-radius conductive wire, which acts as a high-voltage induced corona electrode and two metal plate counter-electrodes. Since it is widely known that positive corona discharge emits much lower ozone concentrations than negative polarity corona [41], positive corona discharge configuration will be preferentially investigated.

The collection stage relies on the migration of the charged particles under the influence of an electric field and their deposition at the surface of collection electrodes. For this purpose, an

electric field is created by applying a potential difference between the collection electrode and a counter-electrode. The selected geometry for the collection stage is a parallel plates configuration.

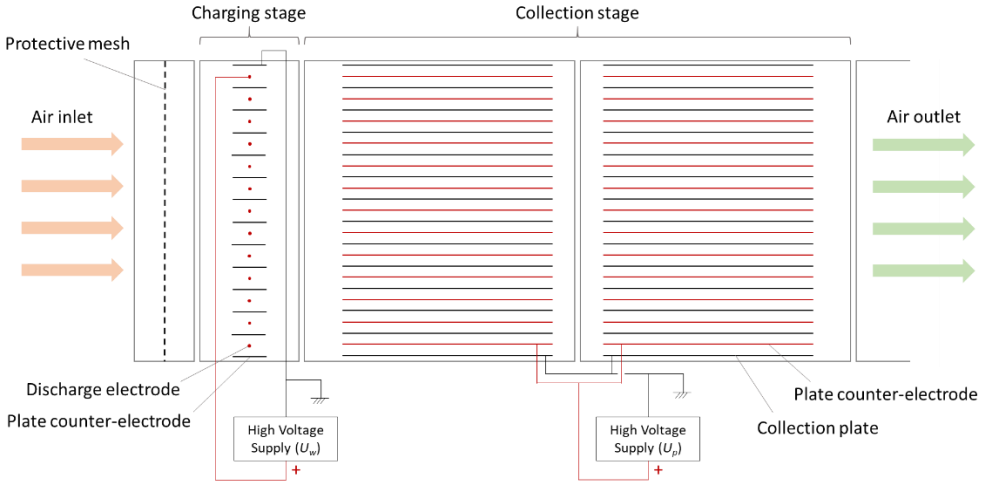

Figure 2. Schematic of the ESP prototype developed in this study.

Final assembly comprises the charging stage and two consecutive collection stages, with an outer section of 355x355 mm^2 and a total length of 640 mm. For the charging stage, the corona discharge is performed using thirteen Ø 80 µm stainless steel wires located at a distance of 10 mm from their plate counter-electrodes. The wires are positively charged, while the counter-electrodes are grounded. The collection stages comprise two sections of 200 mm long copper-coated glass fiber plates, which are alternatively grounded and positively charged. The main specifications of the ESP prototype are summarized in Figure 3 below.

		Charging stage	***Collection stage***
Casing	*Nominal section*	305x305 mm^2	305x305 mm^2
	Length	100 mm	2x270 mm
	Material	Insulated aluminum	Insulated aluminum
Corona wire	*Number*	13	-
	Length	290 mm	-
	Diameter	0.08 mm	-
	Material	Stainless Steel	-
Plates	*Number*	14	2x27
	Length	290 mm	290 mm
	Width	40 mm	200 mm
	Material	Copper-coated glass fiber	Copper-coated glass fiber
***HV* supply**		0-5 kV DC	0-10 kV DC

Figure 3. ESP prototype main specifications and illustration.

Experimental apparatus

Assessment of the single pass particle collection efficiency, pressure drop and ozone emission rate was conducted on a dedicated test rig. This experimental setup was inspired from test equipment for measuring spectral efficiency and air flow resistance of air filters for general ventilation in buildings (as described in EN ISO 16890-2:2016) and of high efficiency air filters (as described in EN 1822-1:2019). The detailed dimensions and constituting elements of the test unit are schematically presented in Figure 4. It comprises a square section (305x305 mm^2)

duct in which the ESP prototype is integrated. The air flow in the duct is controlled by a fan-driven power ventilator equipped with a frequency convertor to adjust speed (airflow rate is monitored with a KIMO AMI 300 propeller anemometer). Unless otherwise specified, the air flowrate in the duct (Q) is fixed at 540 $m^3.h^{-1}$ (corresponding to an airflow velocity of 1.61 $m.s^{-1}$) to match the nominal feed flow of the ESP prototype. This air flowrate was calculated to match the air renewal rate needed for half a cabin of a regional airliner (100 passengers capacity) with a 70% recirculated air ECS design.

The air blower forces the air through an H14 HEPA filter and a concentrated challenge aerosol (generation means are described hereinafter) is mixed with the clean airstream. The airstream charged with the challenge aerosol then passes through the ESP prototype and is collected through the laboratory exhaust system.

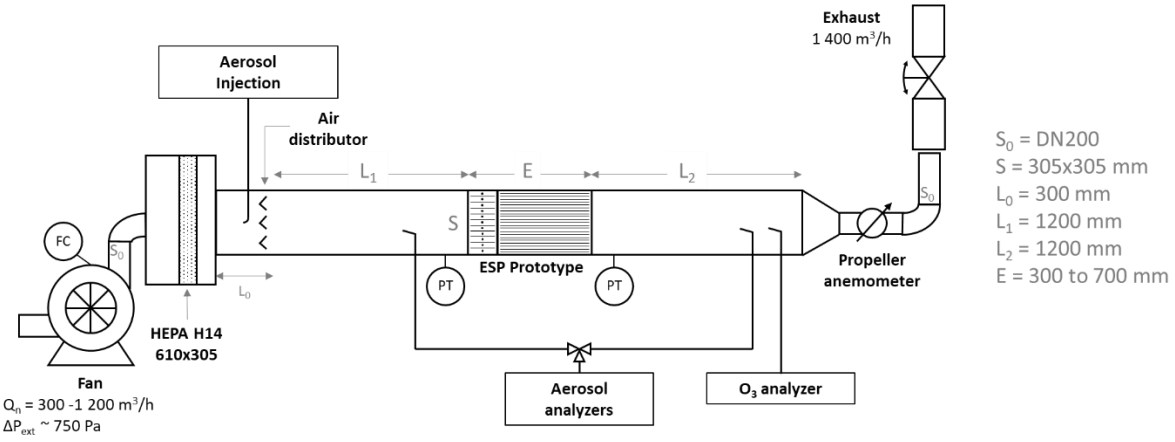

Figure 4. Experimental setup for ESP prototype performance assessment.

The experimental test rig is equipped to monitor in real time:

- The aerosol concentration and size distribution upstream and downstream of the ESP prototype (aerosol characterization means are described hereinafter),
- The ozone concentration downstream of the ESP prototype, using an ENVEA o342e ozone analyzer,
- The ESP prototype pressure drop, using a KIMO AMI 300 manometer.

All the experiments were conducted at 20 ± 2 °C and 45 ± 10% relative humidity.

Challenge aerosols

To produce challenge aerosols with different particle size distributions (PSD), two types of aerosol generators were implemented. After generation, the challenge aerosols were systematically brought to a neutral charge distribution state using an in-house developed neutralizer that produces positive and negative ions by soft X-ray irradiation. Neutralization step effectiveness was confirmed by measuring the neutralized aerosols net charge with a high-capacity Faraday cup aerosol electrometer (PALAS Charme).

Generation of sub-micron and micron sized aerosol was performed using a rotating brush RBG 1000 aerosol generator (PALAS). This equipment produces an aerosol by mechanical solicitation of a powder. The powder to be aerosolized is placed in a container and inserted into

the dispersion head. The powder is then conveyed onto a rotating brush at a precisely controlled feed rate. A compressed air stream tears the particles out of the brush, generating an aerosol at adjustable flowrate. The powder selected for this study is a calibrated calcium carbonate. According to manufacturer specifications, ESKAL 500 (KSL staubtechnik gmbh) is an inorganic mineral powder obtained from natural calcium carbonate ($CaCO_3$) sieved to achieve a narrow particle size distribution (fine and coarse particles are almost eliminated), with a mass based median particle size at approximately 5 µm. When used in the RBG 1000 aerosol generator and after dilution in the clean air stream of the duct, this powder produces a polydisperse aerosol with a number-based PSD (presented in Figure 5-a) ranging from below 500 nm, up to 4 µm (with a mode at approximately 1 µm).

Generation of nano-sized aerosol was performed using a constant output atomizer, model 3076 (TSI). Water vapor is systematically removed from the atomized aerosols using a diffusion dryer (model 6062, TSI). The aerosol precursor for this study is an aqueous sodium chloride (NaCl) solution at a concentration of 1 $g.L^{-1}$. The PSD (recorded by Scanning Mobility Particle Size spectrometer – SMPS) of the aerosol generated from this solution is presented in Figure 5-b. NaCl aerosol number based PSD ranges from below 20 nm, up to 200 nm (with a mode between 40 nm and 45 nm).

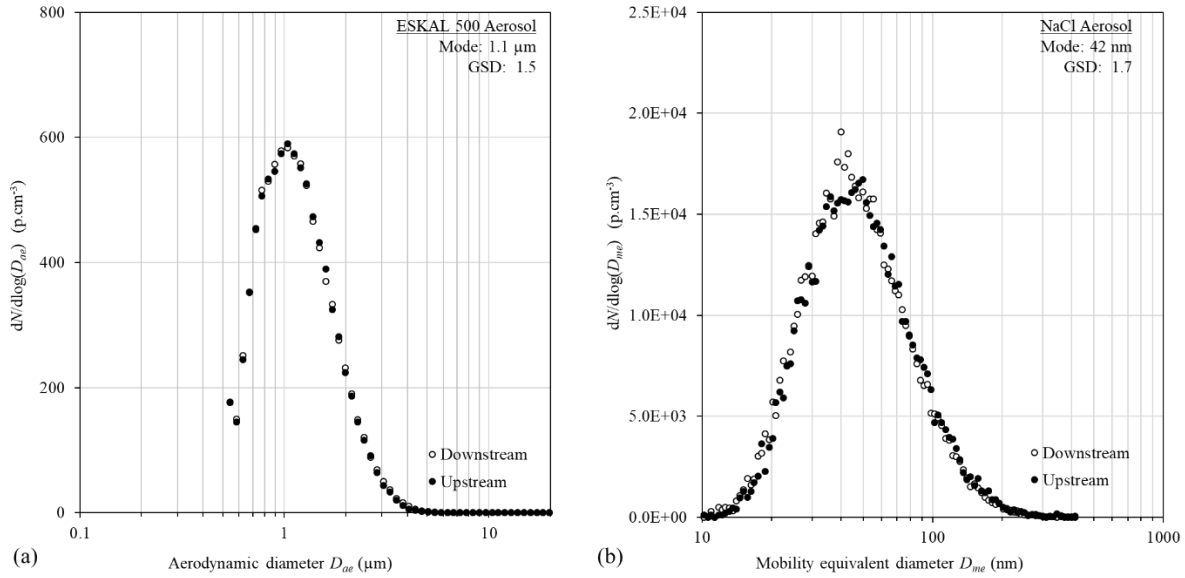

Figure 5. Number-based PSD of (a) ESKAL 500 aerosol (obtained by APS) and (b) NaCl aerosol (obtained by SMPS).

Aerosol characterization and collection efficiency calculation

ESKAL 500 aerosols were monitored using an Aerodynamic Particle Sizer (APS model 3321, TSI). APS relies on particles time-of-flight measurement (using light scattering intensity measurement of two partially overlapping laser beams), providing aerosol concentration and PSD for particle aerodynamic size ranging from 0.5 µm to 20 µm, with a concentration scale from 0.001 $p.cm^{-3}$ up to 1 000 $p.cm^{-3}$. APS operates at 1 Hz sampling rate.

For nano-sized (NaCl) aerosol monitoring, Scanning Mobility Particle Sizer spectrometer (TSI SMPS 3080) was implemented. The SMPS is an electrostatic classifier that comprises a Differential Mobility Analyzer (DMA, TSI 3081) and a Condensation Particle Counter (CPC,

TSI 3785). The DMA separates airborne particles based on their electrical mobility and the CPC optically counts the individual particles (after enlarging them by nucleation growth of droplets in a supersaturated atmosphere). The SMPS provides concentration values and number based PSD for particle size ranging from 5 nm up to 1 000 nm, for concentration values as high as 10^7 p.cm^{-3} [42].

The single-pass particle collection efficiency is obtained by alternatively measuring the particle concentration and PSD upstream and downstream (hereunder respectively referred to as US and DS) of the ESP prototype. More specifically, for ESKAL 500 aerosol challenge, measurement is performed and averaged for 30 s US of the ESP prototype, followed by 30 s DS and another 30 s US to compensate for any concentration change in the test rig. The single-pass particle collection efficiency $\eta(D_p)$ for particles with diameter D_p corresponding to each channel of the spectrometer (SMPS or APS) is then calculated as:

$$\eta(dD_p) = \left(1 - \frac{\overline{N}_{DS}(D_p)}{\frac{\overline{N}_{US1}(D_p)+\overline{N}_{US2}(D_p)}{2}}\right).100 \qquad (1)$$

With: $\overline{N}_{US}(D_p)$ and $\overline{N}_{DS}(D_p)$ the average particle number concentrations for particles with diameter D_p, respectively measured upstream and downstream of the ESP prototype.

Ozone emission rate calculation

Ozone (O_3) concentration change was monitored in the air duct, downstream to the ESP prototype using an ozone analyzer from ENVEA, model o342e. For each set of operational parameters investigated, sampling was performed at 0.1 Hz frequency until reaching steady O_3 concentration for 10 min ($[O_3]_s$). The ozone emission rate (E, in mg.h^{-1}) was then calculated as:

$$E = \frac{([O_3]_s - [O_3]_0).Q.M.P}{R.T}.10^{-3} \qquad (2)$$

With: $[O_3]_0$ the initial ozone O_3 concentration in the air duct (in ppbv), M the molar mass of O_3 (47.998 g.mol^{-1}), P the atmospheric pressure (in Pa), T the temperature in the air duct (in K) and R the universal gas constant (8.314 462 618 J.K^{-1}.mol^{-1}).

RESULTS AND DISCUSSION

Key prototype operating variables were investigated, such as the corona current intensity (I_w) at the charging stage, the plate/plate voltage (U_p) at the collection stage and the filtration air flowrate (Q). The following sections report the results of this parametric study on ESP prototype performances.

To remain in operating conditions that ensure the absence of spark discharge, upper limits were respectively set to 500 µA and 8 kV for corona current intensity (I_w) and plate/plate voltage (U_p). Maximal value of 500 µA for the charging stage I_w was experimentally obtained for a wire/plate voltage (U_w) of 4.9 kV and the positive corona onset voltage was measured at a U_w value of approximately 4.0 kV. The current-voltage and power consumption-voltage characteristic curves are reported in supplementary materials (Figure S1).

Single-pass collection efficiency assessment

Effect of the applied voltage U_p at collection stage

To investigate the influence of U_p on collection efficiency, a series of experiments was conducted. The corona current intensity I_w was set to its maximum value of 500 µA, so that the aerosol challenge particles acquire the highest electrical charge achievable. The airflow Q was maintained at 540 $m^3.h^{-1}$, corresponding to a filtration velocity of 1.61 $m.s^{-1}$.

The ESP prototype was challenged with ESKAL 500 aerosol and the influence of U_p on collection efficiency was assessed for values ranging from 0 kV to 8kV. The spectral collection efficiencies as a function of particle size, obtained in the particle size range of ESKAL 500 aerosol are reported in Figure 6a. The overall ESKAL 500 collection efficiencies (calculated on the overall number based concentrations) are also shown in Figure 6b. The applied U_p has a major influence on collection efficiency, which increased from 14% up to 94% when U_p increased from 0 kV to 8 kV.

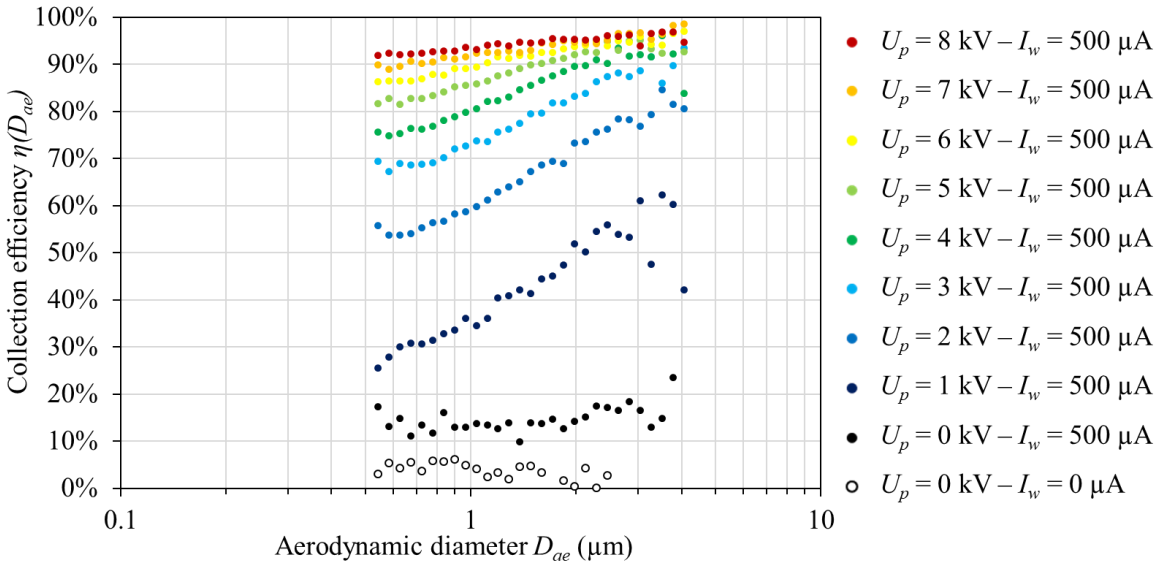

a)

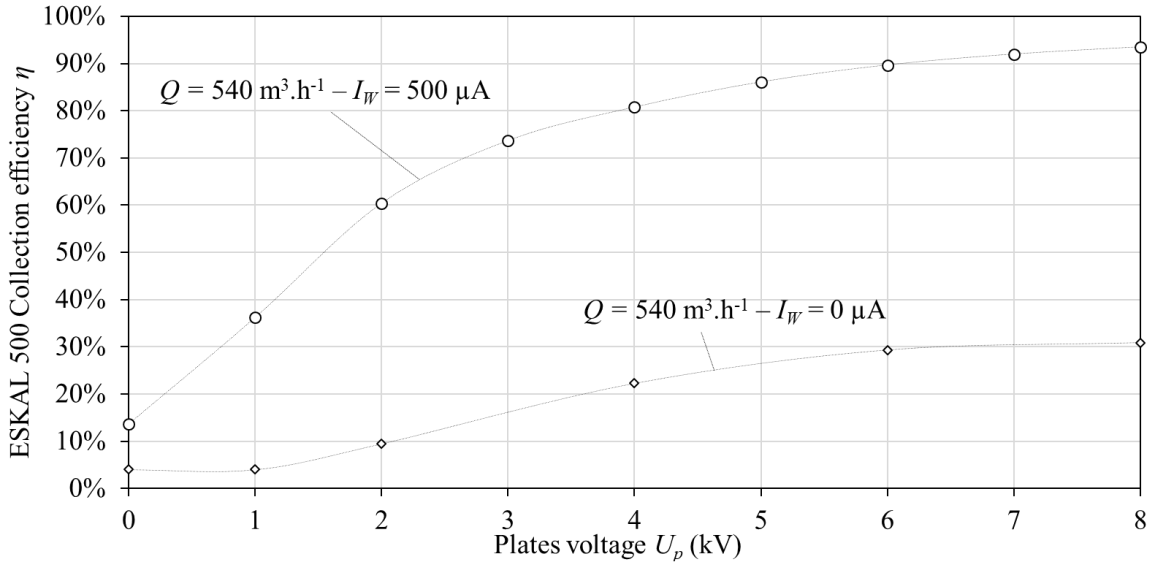

b)

Figure 6. ESP prototype spectral (a) and overall (b) collection efficiencies, for various U_p values (Q = 540 $m^3.h^{-1}$, I_w = 500 µA, ESKAL 500 challenge).

Within particle size range of 500 nm to 4 µm, regardless of the U_p value applied, the spectral efficiencies decrease when the particle size diminishes. This observation is in good agreement with Deutsch-Anderson equation [45] that stipulates that collection efficiency in ESP is driven by particles electrical mobility, which, for micron-sized particles with fixed charging state, decreases with particle size [45]. The spectral efficiencies demonstrate that $PM_{2.5}$ (coarse particles, with an aerodynamic diameter of 2.5 µm and higher) are efficiently filtered (above 90%) for U_p values as low as 4 kV whereas finer particles require U_p to be set above 7 kV to be as efficiently collected.

Effect of corona current I_w at charging stage

To study the effect of corona intensity on particle collection efficiency, U_p was fixed to its maximum value of 8 kV, so that the electric field intensity is maximized at the collection stage, and Q was maintained at 540 $m^3.h^{-1}$.

The ESP prototype was here challenged with both ESKAL 500 and NaCl aerosols, to assess its efficiency on a broad range of particle size (micron/sub-micron sized and UFPs). The spectral collection efficiencies as a function of particle size corresponding to ESKAL 500 aerosol are reported in Figure 7a for positive I_w values (spectral collection efficiencies obtained with negative I_w values are available in supplementary materials, Figure S2). The overall ESKAL 500 collection efficiencies (calculated on the overall number based concentrations) are also shown in Figure 7b. Similarly, spectral and overall collection efficiencies corresponding to NaCl aerosol challenge are respectively reported in Figure 8a and Figure 8b.

For both challenge aerosols, increasing I_w drastically improves the collection efficiency. When I_w was increased from 0 µA to approximately 500 µA, ESKAL 500 and NaCl overall collection efficiencies respectively increased from 29% to 94% and from 45% to 88%. This observation is in agreement with theory since I_w increase generates higher unipolar ion concentrations (N_i), leading to higher charging efficiencies, which is reflected by higher particle collection at fixed U_p. Additionally, one can notice that the ESKAL 500 collection efficiency is substantially higher for positive I_w as compared to equivalent negative I_w.

Analysis of spectral efficiencies obtained for NaCl aerosol challenge shows that, regardless of the I_w applied, the collection efficiency reaches a maximum for particle electrical-mobility diameter between 40 and 80 nm. For smaller particles (20 nm < D_{me} < 40 nm) and for bigger particles (80 nm < D_{me} < 200 nm), the efficiency slightly drops. A most penetrating particle size (MPPS) in the range of 120 nm to 200 nm classically results from the Deutsch-Anderson equation, whereas the efficiency decrease observed for particles below a few tens of nanometers may be attributed to partial charging phenomenon. Indeed Lin et al. [45] suggested a modified Deutsch-Anderson equation accounting for the probability of nanoparticles to hold one elementary charge. This partial charging phenomenon implies that, below 100 nm, an increasing particles fraction remains at neutral state making its collection by electrostatic effect impossible.

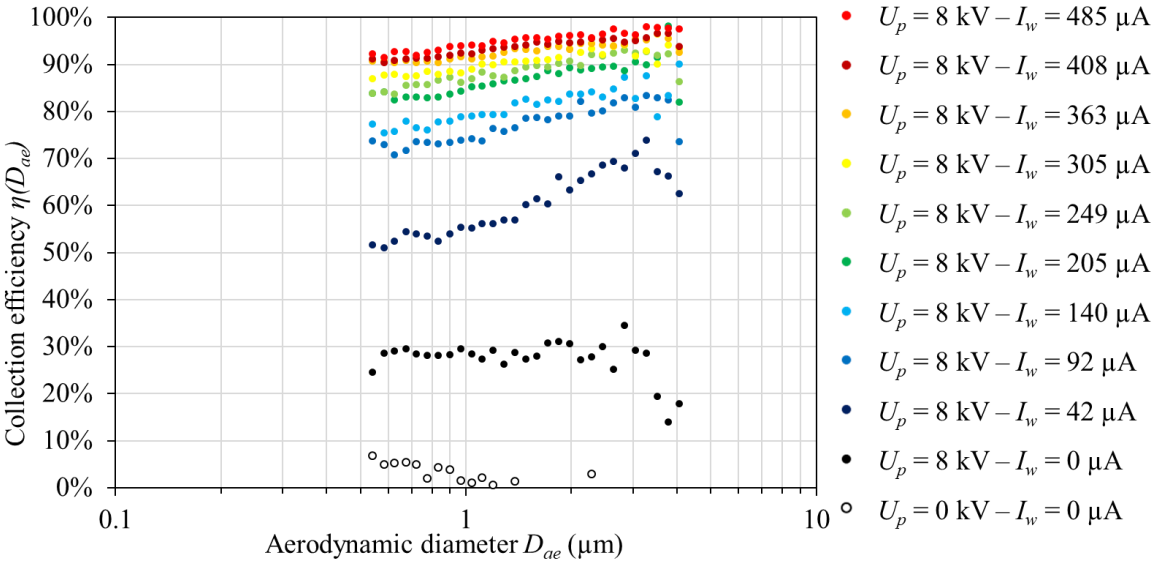

a)

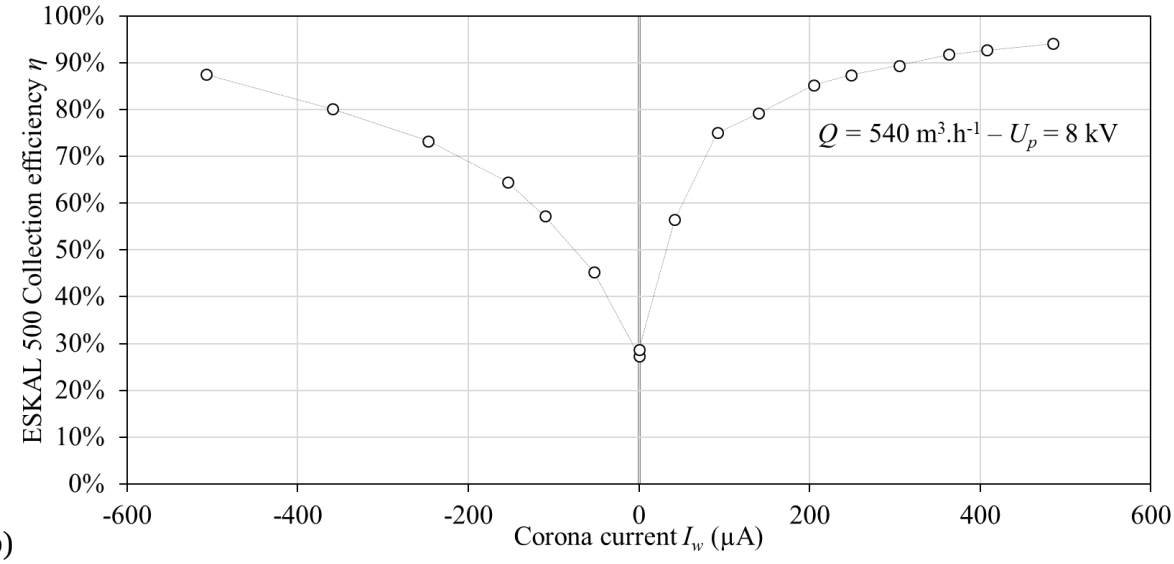

b)

Figure 7. ESP prototype spectral (a) and overall (b) collection efficiencies, for various I_w values (Q = 540 m³.h⁻¹, U_p = 8 kV, ESKAL 500 challenge).

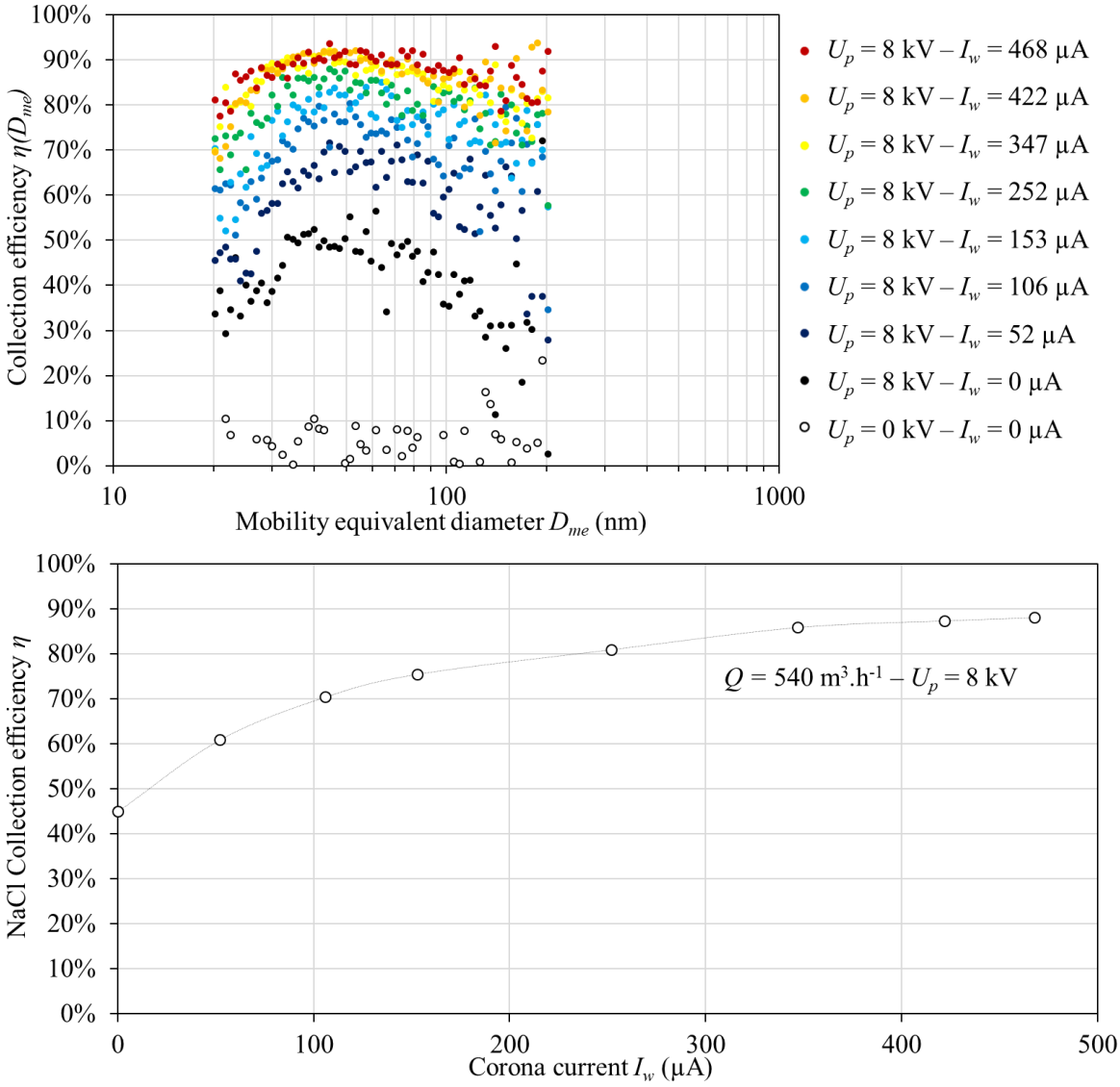

Figure 8. ESP prototype spectral (a) and overall (b) collection efficiencies, for various I_w values (Q = 540 m³.h⁻¹, U_p = 8 kV, NaCl challenge).

Effect of the filtration air flowrate Q

To study the effect of the air velocity on single pass particle collection efficiency, U_p and I_w were fixed at their maximum values (respectively 8 kV and 500 µA).

The ESP prototype was challenged with ESKAL 500 aerosol and the influence of Q on collection efficiency was assessed for values ranging from 120 m³.h⁻¹ to 540 m³.h⁻¹. Spectral efficiencies are presented in Figure 9a and overall efficiencies are reported in Figure 9b. As one can expect, lowering the air flowrate improves the overall system efficiency. When Q decreased from 540 m³.h⁻¹ down to 120 m³.h⁻¹, the single-pass collection efficiency of ESKAL 500 increased from 94% up to over 99.8%. Two distinct phenomena may explain this efficiency improvement: lowering the air velocity in the prototype firstly increases the particles residence time in the charging stage and secondly decreases the tangential component of particles velocity, enabling for more efficient displacement of the particles towards the collection plates.

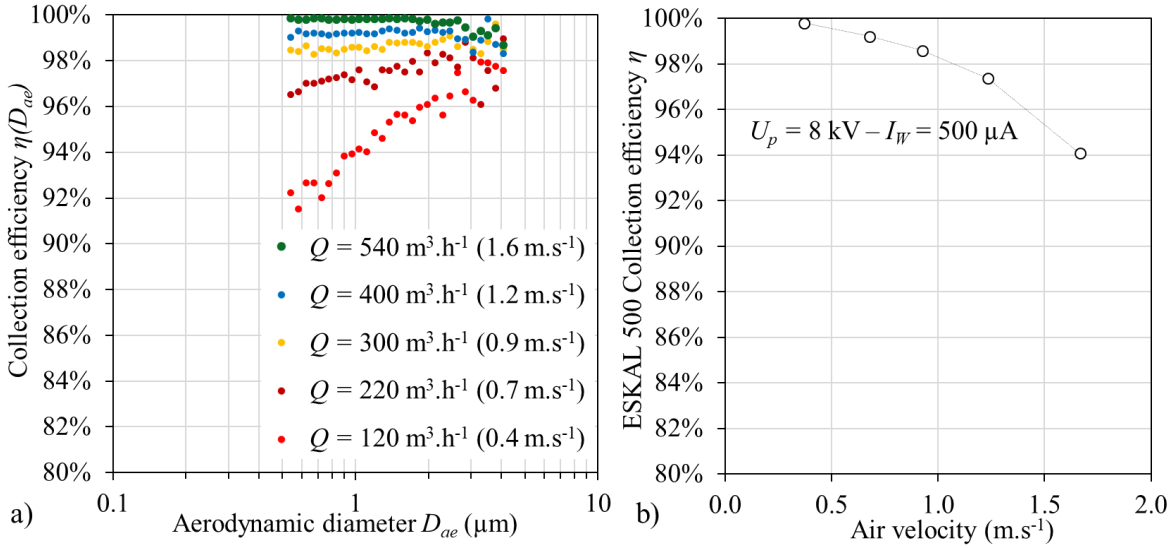

Figure 9. ESP prototype spectral (a) and overall (b) collection efficiencies, for various Q values (U_p = 8 kV, I_w = 500 µA, ESKAL 500 challenge).

Pressure drop assessment

One of the main benefits of ESP over mechanical filtration using non-woven fibrous media filters is its very low theoretical pressure drop, which is beneficial in terms of power consumption. Experimental measurement of the ESP prototype pressure drop was conducted for various air flowrates, as presented in Figure 10. The system pressure drop increases linearly with the air flow and is approximately equal to 4 Pa for the nominal flow rate (540 $m^3.h^{-1}$). ESP pressure drop is therefore 25 to 75 times lower than typical fibrous media filters, which usually exhibit initial pressure drops in the range of 100-300 Pa. Additionally, the ESP system, unlike the fibrous media, does not suffer from pressure drop increase due to fouling and clogging during operation. Indeed, this clogging phenomenon may be considered as the main drawback of fibrous media and can cause pressure drop to be multiplied by up to 10 over the filter lifespan: as reported by Xu et al. [27], the pressure drop of a Donaldson KK2972941 airplane cabin filter was measured at 100 Pa before use and reached 950 Pa after dust loading representative of 6000 flight hours. Nevertheless, additional study will be needed to evaluate the long-term ESP prototype behavior. Indeed, as collected particles accumulate on plates surface, the pressure drop may not significantly change but the efficiency could potentially be impaired due to particles re-entrainment phenomenon [41] (liberation of a fraction of collected particles in the inter-electrode spacing).

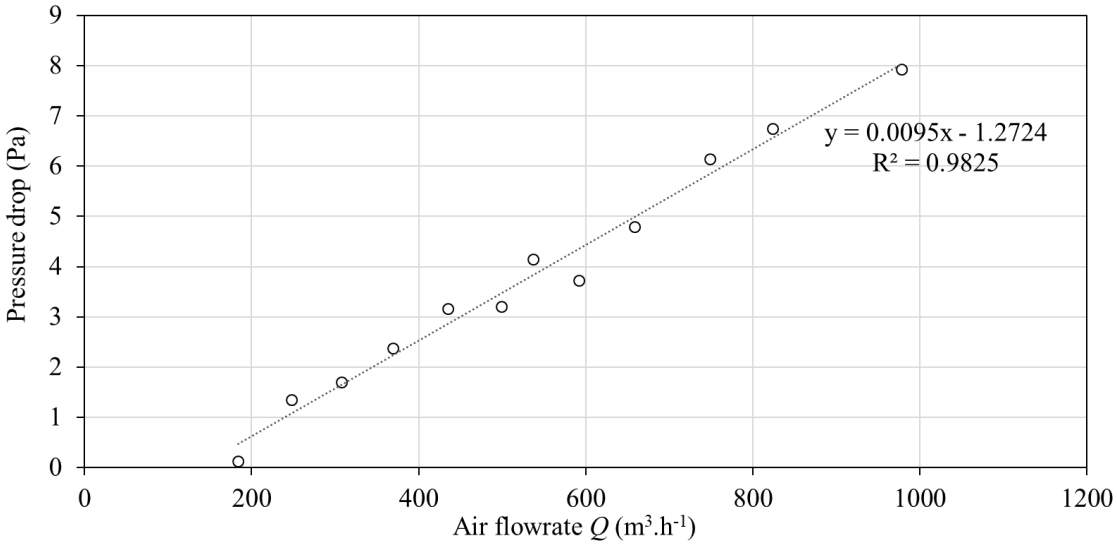

Figure 10. ESP prototype pressure drop as a function of air flowrate Q.

Ozone emission assessment

The ozone generation by corona discharge is a well-recognized phenomenon. Since tropospheric O_3 is considered as an air pollutant [46,47], any device using corona discharge and being used for indoor applications should be designed to ensure that the ozone level does not exceed acceptable limits. For this matter, the ozone emission characteristics of the ESP prototype have been studied for various corona current intensities I_w at charging stage.

Results, expressed in O_3 mass emission rate (E, in mg.h^{-1}) are reported in Figure 11, together with the associated ESKAL 500 collection efficiency. E was found to be directly proportional to I_w ranging from -500 µA to +500 µA. As previously documented [41], E appears to be higher (about 6.6 times) when negative I_w is applied, as compared to positive I_w. The linear relationship between O_3 mass emission rate and positive corona current (in µA) is given by the following relationship: $E = 0.0155*I_w$.

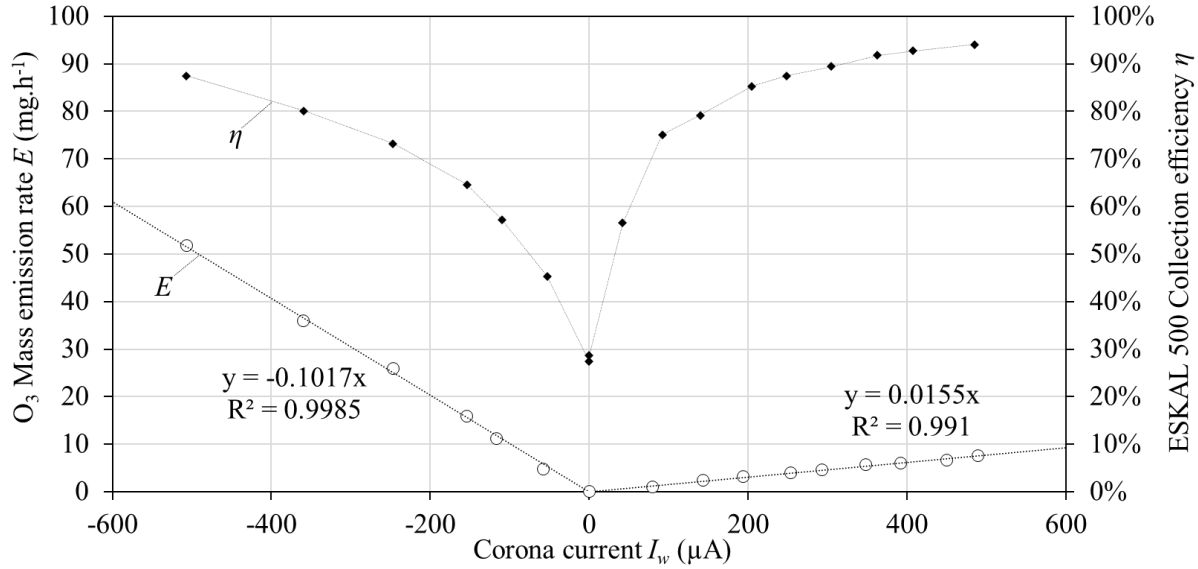

Figure 11. ESP prototype O_3 mass emission rate E and collection efficiency η (with ESKAL 500 challenge), as a function of corona current I_w.

	O_3 mass balance parameters	
Aircraft cabin volume	136	m^3
Recirculation flow Q_r	1080	$m^3.h^{-1}$
Bleed air flow Q_f	460	$m^3.h^{-1}$
Air recycling rate	70	%
Initial [O_3] in the cabin*	28	ppbv
Outside [O_3]*	28	ppbv
Number of ESP devices	2	-
E of one ESP device	8	$mg.h^{-1}$
Final [O_3] (Steady state)	45.4	ppbv

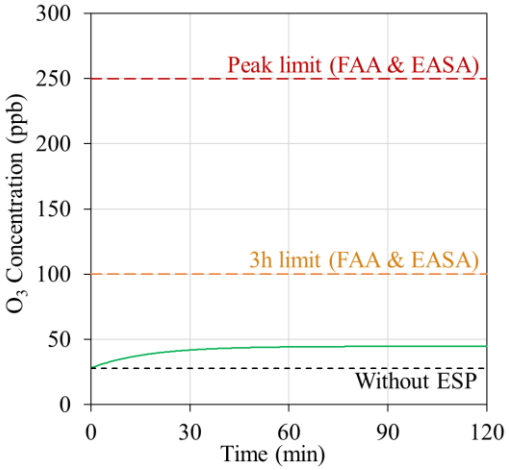

** Maximum recorded mean concentration, according to EASA [48].*

Figure 12. Simulated O_3 concentration change in an aircraft cabin due to ESP operation during flight.

For optimum collection efficiency, the ESP would thus approximately generate 8 $mg.h^{-1}$ of ozone. Considering this value, and using a simplified mass balance model (presented in supplementary materials), calculation can be performed to estimate the O_3 concentration change in an airplane cabin over time. Parameters and results of this calculation are presented in Figure 12. It is worth mentioning that this calculated O_3 concentration increase can be considered as the worst case scenario since it does not take into consideration the influence of natural O_3 decay. Calculation results estimate that the implementation and full-time operation of two ESP prototypes would lead to less than 20 ppbv O_3 increase in the overall aircraft cabin air (in approximately 60 min) of a regional airliner.

CONCLUSION

An ESP prototype sized for aircraft cabin air PM filtration has been successfully designed and its performances in-depth experimentally assessed. The ESP prototype design was made for a half-system, treating half of the total recirculated air flow of a standard regional aircraft cabin (i.e. 540 $m^3.h^{-1}$). The particulate matter collection efficiency as a function of operation parameters (corona current I_w, plate/plate voltage U_p and air flowrate Q) was assessed for nano-, submicron- and micron-sized airborne particles. For nominal operation parameters, a collection efficiency over 90% was demonstrated for airborne particles with an aerodynamic diameter of 0.5 µm or larger. For ultrafine particles (UFP), collection efficiency was assessed at 88% with a NaCl aerosol challenge. The particle charging technology based on corona discharge inherently produces ozone but the optimized design of the ESP prototype was found to limit this unwanted production down to 8 $mg.h^{-1}$, which would induce, even in the worst case scenario, very restrained concentration increase (<20 ppbv) in the aircraft cabin. Lastly, for nominal operation flowrate, the ESP prototype exhibited a pressure drop below 4 Pa, which is 25 to 75 times lower than conventional pristine media filters.

ACKNOWLEDGMENTS

This project has received funding from the Clean Sky 2 Joint Undertaking (CS2JU REG-IAD) under grant agreement No. 831963. The JU receives support from the European Union's Horizon 2020 research and innovation program and the Clean Sky 2 JU members other than the Union.

REFERENCES

[1] Michaelis S., Loraine T., Aircraft Cabin Air Filtration and Related Technologies: Requirements, Present Practice and Prospects. In: Hocking M. (eds) Air Quality in Airplane Cabins and Similar Enclosed Spaces. The Handbook of Environmental Chemistry, 2005, vol. 4H

[2] Pecho P., Škvareková I., Ažaltovič V., Hrúz M., Design of air circuit disinfection against COVID-19 in the conditions of airliners. Transportation Research Procedia, vol. 51, 2020, p. 313-322

[3] Masiol M., Harrison R. M., Aircraft engine exhaust emissions and other airport-related contributions to ambient air pollution: A review, Atmospheric Environment, vol. 95, 2014, p. 409-455

[4] Unal A., Hu Y., Chang M.E., Odman M.T., Russel A.G., Airport related emissions and impacts on air quality: application to the Atlanta International Airport, Atmos. Environ., vol. 39:32, 2005, p. 5787-5798

[5] Song S.-K., Shon Z.-H., Emissions of greenhouse gases and air pollutants from commercial aircraft at international airports in Korea, Atmos. Environ., vol. 61, 2012, p. 148-158

[6] Yang X., Cheng S., Lang J., Xu R., Lv Z., Characterization of aircraft emissions and air quality impacts of an international airport. J. Environ. Sci., vol. 72, 2018, p. 198-207

[7] Marie-Desvergne C., Dubosson M., Touri L., Zimmermann E., Gaude-Môme M., Leclerc L., Durand C., Klerlein M., Molinari N., Vachier I., Chanez P. and Chamel Mossuz V., Assessment of nanoparticles and metal exposure of airport workers using exhaled breath condensate, J. Breath Res., vol. 10:3, 2016, 036006

[8] Lobo P., Durdina L., Smallwood G. J., Rindlisbacher T., Siegerist F., Black E. A., Yu Z., Mensah A. A., Hagen D. E., Miake-Lye R. C., Thomson K. A., Brem B. T., Corbin J. C., Abegglen M., Sierau B., Whitefield P. D. & Wang J., Measurement of Aircraft Engine Non-Volatile PM Emissions: Results of the Aviation-Particle Regulatory Instrumentation Demonstration Experiment (A-PRIDE) 4 Campaign, Aerosol Science and Technology, vol. 49:7, 2015, p. 472-484

[9] Stacey B., Harrison R. M., Pope F., Evaluation of ultrafine particle concentrations and size distributions at London Heathrow Airport, Atmospheric Environment, vol. 222, 2020, 117148

[10] Austin E., Xiang J., Gould T. R., Shirai J. H., Yun S., Yost M. G., Larson T. V., and Seto E., Distinct Ultrafine Particle Profiles Associated with Aircraft and Roadway Traffic, Environ. Sci. Technol., vol. 55:5, 2021, p. 2847-2858

[11] Zhu Y., Fanning E., Yu R. C., Zhang Q., Froines J. R., Aircraft emissions and local air quality impacts from takeoff activities at a large International Airport, Atmospheric Environment, vol. 45:36, 2011, p. 6526-6533

[12] De Reus M., Ström J., Hoor P., Lelieveld J., Schiller C., Particle production in the lowermost stratosphere by convective lifting of the tropopause, J. Geophys. Res. Atmospheres, vol. 104:19, 1999, p. 23935-23940

[13] Hofzumahaus A., Rohrer F., Lu1 K., Bohn B., Brauers T., Chang C.-C., Fuchs H., Holland F., Kita K., Kondo Y., Li X., Lou S., Shao M., Zeng L., Wahner A., Zhang Y., Amplified Trace Gas Removal in the Troposphere, Science, vol. 324:5935, 2009, p. 1702-1704

[14] Bhangar S. and Nazaroff W. W., Atmospheric ozone levels encountered by commercial aircraft on transatlantic routes, Environ. Res. Lett., vol. 8:1, 2013, 014006

[15] Marenco A., Measurement of ozone and water vapor by Airbus in-service aircraft: The MOZAIC airborne program, An overview, 1998

[16] EASA.2015.HVP.23: Characterisation of the toxicity of aviation turbine engine oils after pyrolysis (AVOIL) , 2017

[17] Michaelis S., « Oil bearing seals and aircraft cabin air contamination », 2016.

[18] Schuchardt S., Koch W. & Rosenberger W., Cabin air quality – Quantitative comparison of volatile air contaminants at different flight phases during 177 commercial flights, Build. Environ., vol. 148, 2019, p. 498-507

[19] National Research Council (US) Committee on Air Quality in Passenger Cabins of Commercial Aircraft, The Airliner Cabin Environment and the Health of Passengers and Crew. Washington (DC): National Academies Press (US); 2002. COMMITTEE ON AIR QUALITY IN PASSENGER CABINS OF COMMERCIAL AIRCRAFT. Available from: https://www.ncbi.nlm.nih.gov/books/NBK207478/. National Academies Press (US), 2002

[20] Cao Q., Chen C., Liu S., Lin, C.-H. Wei D., Chen Q., Prediction of particle deposition around the cabin air supply nozzles of commercial airplanes using measured in-cabin particle emission rates, Indoor Air, vol. 28:6, 2018, p. 852-865

[21] Spengler J. D., Vallarino J., McNeely E., Estephan H., Sumner A. L., In-flight/onboard monitoring: ACER's component for ASHRAE 1262, Part 2, Boston RITEACER RITE-ACER-CoE-2012-6, 2012

[22] EASA_REP_RESEA_2014_4 CAQ Preliminary cabin air quality measurement campaign, 2017

[23] Guan J., Jia Y., Wei Z., Tian X., Temporal variations of ultrafine particle concentrations in aircraft cabin: A field study, Build. Environ., vol. 153, 2019, p. 118-127

[24] Nagda N. L., Koontz M. D., Konheim A. G., Katharine Hammond S., Measurement of cabin air quality aboard commercial airliners, Fifth Int. Conf. Indoor Air Qual. Clim. Indoor Air 90 Charact. Indoor Air, vol. 26:12, 1992, p. 2203-2210

[25] Cheng X., Tan Z., Tay R., Yuan W., Air Quality in transport cabin- Part I, ASHRAE Trans., vol. 112, 2006, p. 505

[26] Lee S.-C., Poon C.-S., Li X.-D., Luk F., Indoor air quality investigation on commercial aircraft, Indoor Air, vol. 9:3, 1999, p. 180-187

[27] Xu B., Liu J., Ren S., Yin W., Chen Q., Investigation on the performance of airliner cabin air filter throughout the lifetime usage, Aerosol and Air Quality Research, vol. 13, 2013, p. 1544-1551

[28] Michaelis S., Health and Flight Safety Implications from Exposure to Contaminated Air in Aircraft, PhD Thesis, University of New South Wales, 2010

[29] Podgórski A., Bałazy A., Gradoń L., Application of nanofibers to improve the filtration efficiency of the most penetrating aerosol particles in fibrous filters, Chemical Engineering Science, vol. 61, 2006, p. 6804-6815

[30] Kettleson E., Schriewer J., Buller R., Biswas P., Soft-X-Ray-Enhanced Electrostatic Precipitation for Protection against Inhalable Allergens, Ultrafine Particles, and Microbial Infections, Appl Environ Microbiol., vol. 79:4, 2013, p. 1333-1341

[31] Jaworek A., Krupa A., Czech T., Modern electrostatic devices and methods for exhaust gas cleaning: A brief review, Journal of Electrostatics, vol. 65, 2007, p. 133-155

[32] Wen T., Krichtafovitch I., Mamishev A., The key energy performance of novel electrostatic precipitators, Journal of Building Engineering, vol. 2, 2015, p. 77–84

[33] Kim M., Lim G.-T., Kim Y.-J., Han B., Woo C. G., Kim H.-J., A novel electrostatic precipitator-type small air purifier with a carbon fiber ionizer and an activated carbon fiber filter, Journal of Aerosol Science, vol. 117, 2018, p. 63-73

[34] Liu G., Xiao M., Zhang X., Gal C., Chen X., Liu L., Pan S., Wu J., Tang L., Clements-Croome D., A review of air filtration technologies for sustainable and healthy building ventilation, Sustainable Cities and Society, vol. 32, 2017

[35] Mittal H., Parks S., Pottage T., Walker J., Bennett A., Survival of Microorganisms on HEPA Filters, Applied Biosafety, vol. 16:.3, 2011

[36] Mainelis G., Górny R., Reponen T., Trunov M., Grinshpun S., Baron P., Yadav J., Willeke K., Effect of electrical charges and fields on injury and viability of airborne bacteria, Biotechnol. Bioeng., vol.79,2002, p.229-241

[37] Yao M., Mainelis G., An H., Inactivation of Microorganisms Using Electrostatic Fields, Environ. Sci. Technol., vol. 39:9, 2005, p. 3338-3344

[38] ANSES, Identification et Analyse des Différentes Techniques d'Epuration d'Air Intérieur Emergentes, Rapport d'expertise collective, ISBN 979-10-286-0173-7, 2017

[39] Afshari A., Ekberg L., Forejt L., Mo J., Rahimi S., Siegel J., Chen W., Wargocki P., Zurami S., Zhang J., Electrostatic Precipitators as an Indoor Air Cleaner - A Literature Review, Sustainability, vol. 12:21, 2020, 8774

[40] Chen L., Gonze E., Ondarts M., Outin J., Gonthier Y., Electrostatic precipitator for fine and ultrafine particle removal from indoor air environments, Separation and Purification Technology, vol. 247, 2020, 116964

[41] Mizuno A., Electrostatic Precipitation, IEEE Trans. Dielectr. & Electr. Insul., vol. 7:5, 2000, p.615-624

[42] Asbach C., Clavaguera S., Todea A. M., Measurement Methods for Nanoparticles in Indoor and Outdoor Air, Indoor and Outdoor Nanoparticles: The Handbook of Environmental Chemistry, vol. 48, 2015, p. 19-49

[43] Huang Y. et al., Recent Progress of Dry Electrostatic Precipitation for PM2.5 Emission Control from Coal-fired Boilers, Int. J. Plasma Environ. Sci. Technol., vol. 9:2, 2015, p. 69-95

[44] Lawless P. A., Particle charging bounds, symmetry relations, and an analytic charging rate model for continuum regime, J Aerosol Sci, vol. 27:2, 1996, p. 191-215

[45] Lin G. Y., Chen T. M., Tsai C. J., A Modified Deutsch-Anderson Equation for Predicting the Nanoparticle Collection Efficiency of Electrostatic Precipitators, Aerosol Air Qual. Res., vol. 12:5, 2012, p. 697-706

[46] USEPA, Air Quality Criteria for Ozone and Related Photochemical Oxidants (Final Report), U.S. Environmental Protection Agency, EPA/600/R-05/004aF-cF, 2006

[47] Health Risks of Ozone from Long-range Transboundary Air Pollution, World Health Organisation, 2008

[48] EASA. Preliminary cabin air quality measurement campaign (CAQ)EASA.2014.C15 and (CAQII)EASA.2014.C15.SU01, 2014

SUPPLEMENTARY MATERIALS

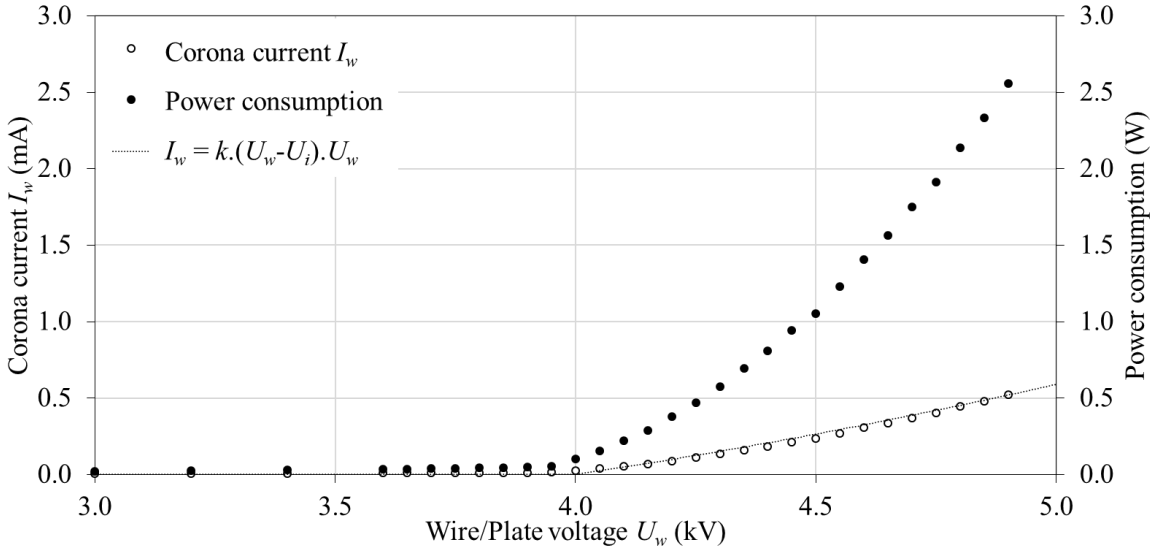

Figure S1. Current-voltage and power consumption-voltage characteristic curves.

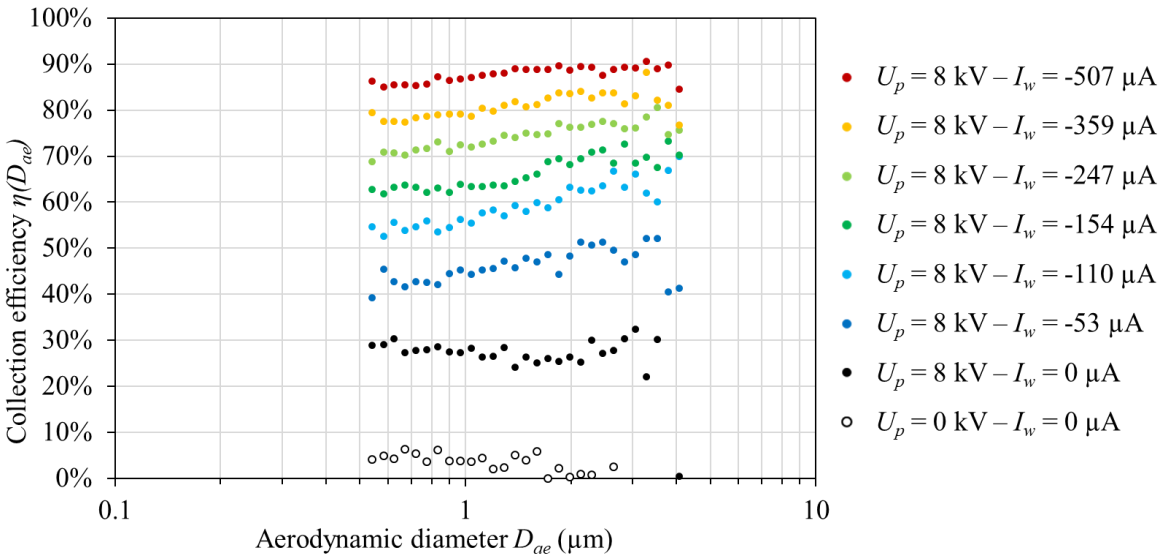

Figure S2. ESP prototype spectral collection efficiencies, for various I_w negative values (Q = 540 m^3.h^{-1}, U_p = 8 kV, ESKAL 500 challenge).

Details of the simplified mass balance model to simulate [O_3] and PM in an airplane cabin

The model considers a medium size regional airliner cabin volume V of 136 m^3, accommodating for 100 passengers. Fresh air is supplied to the cabin with a flowrate Q_f, while the air inside the cabin is recirculated and filtered with a total flowrate Q_r according to the Figure S3 below. The cabin is assumed to be pressurized at the atmospheric pressure and thermalized at 20 °C.

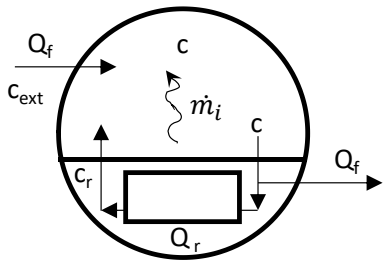

Figure S3. Simplified diagram of the air supply system.

The air in the cabin is assumed to be well mixed, so that the pollutant concentration (PM or O_3) is essentially uniform and equal to a single value c. This assumption is quite common (see for instance the model for PM in [20]) and allows to ignore the complex air flow pattern in the cabin. With this assumption, the pollutant mass balance in the cabin reads:

$$V\frac{dc}{dt} = Q_f c_{ext} + \dot{m}_i + Q_r c_r - \left(Q_f + Q_r\right)\mathrm{c} \qquad \text{(S.1)}$$

Where:
- c_{ext} is the outside pollutant concentration
- $\dot{m}_i$ is the internal pollutant source
- c_r is the concentration at the outlet of the filters.

For consistency, in this equation flowrates are expressed in $m^3.s^{-1}$, concentrations in $kg.m^{-3}$ and sources in $kg.s^{-1}$. All are evaluated under cabin temperature and pressure conditions.

Simulation of ESP operation on [O_3] in the airplane cabin

O_3 emission by the ESP prototype operation is assimilated here to the O_3 internal pollution source $\dot{m}_i$. For this simulation, to be able to discriminate the impact of ESP operation on [O_3] in the cabin, the outside O_3 concentration (c_{ext}) is set as a constant, and the higher O_3 concentrations that may be found at high altitudes are considered to be regulated by the presence of an airplane ozone scrubber located on the bleed airflow path. Other potential contamination sources and the O_3 natural decay inside the cabin are neglected. Since the O_3 produced by the ESP is accounted for as internal pollution source (in other words: $c_r = c$), the mass balance equation can be simplified as follows:

$$V\frac{dc}{dt} = Q_f(c_{ext} - c) + \dot{m}_i \qquad \text{(S.2)}$$

The solution of this simplified equation is then calculated as:

$$c = c_{ext} + \frac{\dot{m}_i}{Q_f}\left(1 - exp\left(-\frac{Q_f t}{V}\right)\right) \qquad \text{(S.3)}$$

Selected parameters and resulting influence of ESP prototype operation on [O_3] in an airplane cabin (calculated from equation S.3) are reported on Figure 12.

Simulation of ESP operation on PM in the airplane cabin

The same model can be used to evaluate the impact of filter efficiency on PM concentration in the cabin over time. Since PM concentration on the tarmac may reach very high concentrations, the worst situations for PM pollution are the ground operations such as taxiing. Here the internal PM pollution source $\dot{m}_i$ can be neglected and c_r is defined through the PM filter single-pass efficiency. The mass balance equation may then be expressed as:

$$V\frac{dc}{dt} = Q_f c_{ext} - \mathrm{c}\left(Q_r\eta + Q_f\right) \quad \text{(S.4)}$$

Considering an initial PM concentration in the airplane cabin c_i, the solution of this simplified equation can then be calculated as:

$$\mathrm{c(t)} = c_i.\exp\left(-\frac{(Q_r\eta+Q_f)t}{V}\right) + \frac{Q_f c_{ext}}{(Q_r\eta+Q_f)}\left(1-\exp\left(-\frac{(Q_r\eta+Q_f)t}{V}\right)\right) \quad \text{(S.5)}$$

Using (S.5), the PM concentration change as a function of time can be calculated for various filter efficiencies. Figure S4 presents the PM concentration change in an airplane cabin during a phase (such as landing and taxiing) where the initial concentration in the plane (fixed at 100 p.cm^{-3}) is substantially lower than the outside concentration (fixed at 100 000 p.cm^{-3}). In this situation, the cabin PM concentration rapidly increases. Without filtering system, PM concentration in the cabin would tend to increase until equalizing the outside concentration. With the implementation of a filter, the increase would be contained at a level that depends on the filter efficiency. A 99.9% efficiency HEPA filter would limit the concentration in the cabin at 30 081 p.cm^{-3}, while the implementation of the ESP prototype developed in this study (94% PM_{10} efficiency and 88% UFP efficiency) would maintain concentration in the range of 31 182 to 32 615 p.cm^{-3}. Those steady state concentrations are reached within approximately 30 min. In this situation, replacing an HEPA filter by the ESP prototype would lead to a concentration increase in the airplane cabin by at most 3.7% (PM_{10}) to 8.4% (UFP).

		PM mass balance parameters		
Aircraft cabin volume		136		m^3
Recirculation flow Q_r		1080		$m^3.h^{-1}$
Bleed air flow Q_f		460		$m^3.h^{-1}$
Air recycling rate		70		%
Initial [PM] in the cabin, c_i		10^2		$p.cm^{-3}$
Outside [PM], c_{ext}		10^5		$p.cm^{-3}$
PM filter efficiency	99.9	94	88	%
Final [PM] (Steady state)	30 081	31 182	32 615	$p.cm^{-3}$

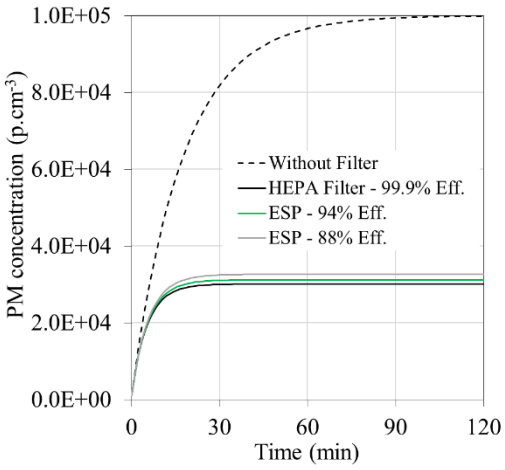

Figure S4. Simulated PM concentration change in an aircraft cabin for different filter efficiencies during on-ground operation.

It is worth mentioning that the described scenario points out the limitations of the ECS design implemented on nowadays airliner, with the absence of bleed air filtration before being mixed with the recirculated air.